

Vlasov-Maxwell, self-consistent electromagnetic wave emission simulations in the solar corona

David Tsiklauri¹

© Springer ●●●

Abstract 1.5D Vlasov-Maxwell simulations are employed to model electromagnetic emission generation in a fully self-consistent plasma kinetic model for the first time in the solar physics context. The simulations mimic the plasma emission mechanism and Larmor drift instability in a plasma thread that connects the Sun to Earth with the spatial scales compressed appropriately. The effects of spatial density gradients on the generation of electromagnetic radiation are investigated. It is shown that 1.5D inhomogeneous plasma with a uniform background magnetic field directed transverse to the density gradient is aperiodically unstable to Larmor-drift instability. The latter results in a novel effect of generation of electromagnetic emission at plasma frequency. The generated perturbations consist of two parts: (i) non-escaping (trapped) Langmuir type oscillations which are localised in the regions of density inhomogeneity, and are highly filamentary, with the period of appearance of the filaments close to electron plasma frequency in the dense regions; and (ii) escaping electromagnetic radiation with phase speeds close to the speed of light. When density gradient is removed (i.e. when plasma becomes stable to Larmor-drift instability) and a *low density* super-thermal, hot beam is injected along the domain, in the direction perpendicular to the magnetic field, plasma emission mechanism generates non-escaping Langmuir type oscillations which in turn generate escaping electromagnetic radiation. It is found that in the spatial location where the beam is injected, the standing waves, oscillating at the plasma frequency, are excited. These can be used to interpret the horizontal strips (the narrowband line emission) observed in some dynamical spectra. Quasilinear theory predictions: (i) the electron free streaming and (ii) the beam long relaxation time, in accord with the analytic expressions, are corroborated via direct, fully-kinetic simulation. Finally, the interplay of Larmor-drift instability and plasma emission mechanism is studied by considering *dense* electron beam in the Larmor-drift unstable (inhomogeneous) plasma. The latter case enables one to study the deviations from the quasilinear theory.

Keywords: Corona, Radio Emission; Radio Emission, Theory; Energetic Particles, Electrons, Acceleration; Flares, Energetic Particles; Instabilities; Magnetic fields, Corona

¹Astronomy Unit, School of Mathematical Sciences, Queen Mary University of London, Mile End Road, London, E1 4NS, United Kingdom

1. Introduction

The aim of this paper is to employ Vlasov-Maxwell simulations for the electromagnetic wave generation by a super-thermal ($0.2 - 0.5c$), hot electron beam injected into the solar coronal magnetised plasma. Since such beams are thought to be responsible for the generation of type III solar radio bursts we start from a brief review of the previous relevant results. Although we stress that for the reasons described below, at this stage, the model presented here cannot be directly applied to the type III bursts and it is perhaps more relevant for the interpretation of the narrowband line emission observations. The type III solar radio bursts are believed to come from the super-thermal beam of electrons that travel away from the Sun producing the observed electromagnetic (EM) radiation via the plasma emission mechanism (see e.g. Melrose, Nindos *et al.*, Pick and Vilmer, 1987, 2008, 2008 for recent reviews). Basic physical understanding of the generation of type III radio burst EM waves in plasma by an electron beam has been with us for over five decades (Ginzburg and Zhelezniakov, 1958) and involves the generation of Langmuir waves by bump-on-tail unstable electron distributions and subsequent mode conversion of the longitudinal Langmuir waves into escaping, transverse EM radiation. Theoretical efforts in understanding of type III solar radio bursts can be grouped into three categories:

(1) Quasilinear theory of type III sources that use kinetic Fokker-Planck type equation for describing the dynamics of an electron beam, coupled with spectral energy density evolutionary equations for Langmuir and ion-sound waves have long been studied. The most essential result is that the spectral energy density of the Langmuir wave packets (that are excited by the bump-on-tail unstable beam) travels along the open magnetic field lines with a constant speed and this is despite the quasilinear relaxation (formation of a plateau in the longitudinal, along the beam injection direction, velocity phase-space of the electron distribution function), hence, this implies some sort of beam marginal stabilisation (Kaplan and Tsytovich, 1968; Smith, 1970; Zaitsev, Mityakov, and Rapoport, 1972; Mel'Nik, Lapshin, and Kontar, 1999; Kontar and Pécseli, 2002). Inclusion of EM emission component into the quasilinear theory in some models is based on so-called drift approximation (Hillaris, Alissandrakis, and Vlahos, 1988; Hillaris *et al.*, 1990; Hillaris *et al.*, 1999), where nonlinear beam stabilisation during its propagation (so called free streaming) is based on Langmuir-ion acoustic wave coupling via ponderomotive force and EM emission is prescribed by a power law of the beam to ambient plasma number density ratio. These models can be successfully compared with the observed dynamical spectra to constrain key model parameters.

(2) Stochastic growth theory (Robinson, 1992; Robinson, Cairns, and Gurnett, 1992), in which density irregularities induce random growth, such that Langmuir waves are generated stochastically and quasilinear interactions within these Langmuir clumps cause the beam to fluctuate about marginal stability. Further this approach has been developed into a numerical simulation tool that effectively can reproduce observational features of the type III bursts (Li, Cairns, and Robinson, 2008).

(3) Full kinetic simulation approach of type III bursts (Kasaba, Matsumoto, and Omura, 2001; Sakai, Kitamoto, and Saito, 2005; Rhee *et al.*, 2009; Umeda, 2010) to this date

used Particle-In-Cell (PIC) numerical method. This effort is mainly focused on understanding of basic physics rather than direct comparison with the observations because the size of simulation domain of the models corresponds to only few 1000 Debye lengths which is roughly $1/10^{10}$ th of 1 AU. Thus, such models deal with micro-scales.

Each of the above theoretical approaches have their advantages and disadvantages. For example as it is well explained in Cairns (1985), in quasilinear theory the particle distribution function is split into a slowly varying average part and a rapidly varying part due to a wave. Then major approximation is that interactions between wave modes are neglected and only back-reaction of the waves on the slowly varying average part of the distribution function is considered. Therefore, if computational resources permit, the full kinetic approach is more desirable. However, to this date only PIC method was used. It is well known that PIC approach suffers from large, so called, "shot-noise" level of which scales as one over the root of number of particles. Moreover, in PIC approach typically there are few hundred particles per cell (which is normally one Debye length long in fully electromagnetic PIC codes). In Vlasov-Maxwell approach instead of solving for individual particle dynamics, without loss of generality (or any kinetic physics), collisionless Vlasov equation for electrons and ions is solved in which EM fields are self-consistent. In this study we use 80×80 velocity grid which in PIC equivalent would be having $80 \times 80 = 6400$ particles per cell (instead of few hundred). We have also done convergence tests by increasing the resolution both in velocity space and spatial domain and confirmed the results' convergence. This shows that Vlasov-Maxwell approach probes more finely phase space of the problem but this comes at a substantial memory cost.

The paper is organised as following. In Section 2 we present the model and main results, including (i) a numerical run of the inhomogeneous plasma without a beam which turns out to be aperiodically unstable to a Larmor drift. The latter results in Langmuir and EM wave generation, as well as density filamentation (Section 2.1); (ii) a numerical run of the homogeneous plasma with a low density beam which generates Langmuir and EM wave via plasma emission mechanism (Section 2.2); and a numerical run of the inhomogeneous plasma with a high density beam in order to combine the effects of both density inhomogeneity and the presence of the beam (Section 2.3).

2. The model and general theoretical considerations

Our numerical model is implemented using a relativistic, fully electromagnetic Vlasov-Maxwell code called VALIS (Sircombe and Arber, 2009). The code is using a conservative, split-Eulerian scheme based on the Piecewise Parabolic Method for the update of the particle distribution function and utilising the exact particle fluxes to calculate the current in the solution of Maxwell's equations. In particular relativistic Vlasov's equation is solved for species α ($\alpha = e, i$ for electrons and ions respectively)

$$\frac{\partial f_\alpha}{\partial t} + \frac{\mathbf{u}}{\gamma^*} \cdot \nabla_x f_\alpha + \frac{q_\alpha}{m_\alpha} \left(\mathbf{E} + \frac{\mathbf{u}}{\gamma^*} \times \mathbf{B} \right) \cdot \nabla_{\mathbf{u}} f_\alpha = 0 \quad (1)$$

in conjunction with the Maxwell's equations

$$\nabla \cdot \mathbf{E} = \rho/\varepsilon_0, \quad \nabla \cdot \mathbf{B} = 0, \quad \nabla \times \mathbf{E} = -\frac{\partial \mathbf{B}}{\partial t}, \quad \nabla \times \mathbf{B} = \mu_0 \mathbf{J} + \frac{1}{c^2} \frac{\partial \mathbf{E}}{\partial t}, \quad (2)$$

where charge and current densities are specified in *self-consistent* manner,

$$\rho = \sum_{\alpha} q_{\alpha} \int f_{\alpha} d^3u, \quad \mathbf{J} = \sum_{\alpha} q_{\alpha} \int (\mathbf{u}/\gamma^*) f_{\alpha} d^3u, \quad (3)$$

and $\gamma^* = \sqrt{1 + |\mathbf{u}|^2/c^2}$.

VALIS is 2D2V code in that it has two spatial dimensions (x, y) and two corresponding velocity components (u_x, u_y) , while electric and magnetic field components that are solved for are $(E_x, E_y, 0)$ and $(0, 0, B_z)$. Distance and time are normalised to c/ω_{pe} and ω_{pe}^{-1} , while electric and magnetic fields to $\omega_{pe} c m_e/e$ and $\omega_{pe} m_e/e$ respectively. Temperature is normalised to $m_e c^2/k$. Here $\omega_{pe} = \sqrt{n_e e^2/(\varepsilon_0 m_e)}$ is the electron plasma frequency, $n_{\alpha} = \int f_{\alpha} d^3u$ is the number density and all other symbols have their usual meaning.

We intend to consider a single plasma thread (i.e. to use 1.5D geometry), therefore space components considered are $(x, y) = (25000\lambda_D, 1\lambda_D)$ with $\lambda_D = v_{th,e}/\omega_{pe}$ being Debye length (here $v_{th,e} = \sqrt{kT/m_e}$ is electron thermal speed). We would like to resolve full plasma kinetics, therefore we set spatial grid size as $1\lambda_D$. In practice this means we set plasma temperature at $T = 10^5\text{K}$ (i.e. fix $v_{th,e}$ at $4.12 \times 10^{-3}c$), which corresponds to high solar corona, above active regions. In the presented results (and in the VALIS code generally) spatial scales are normalised to c/ω_{pe} . We do not fix plasma number density and hence ω_{pe} deliberately, because we wish our results to stay general. In order to achieve this generality (and consistency of the results) it is important to keep normalised $\bar{B}_{z0} = B_{z0}/(\omega_{pe} m_e/e) = 0.01$ the same in all numerical runs. Because B_{z0} is normalised to $\omega_{pe} m_e/e$, no matter how plasma density and hence ω_{pe} changes, (i) ratio of Debye length and c/ω_{pe} , i.e. $\lambda_D/(c/\omega_{pe}) = 4.12 \times 10^{-3}$ and ratio of electron Larmor radius and c/ω_{pe} , i.e. $r_{L,e}/(c/\omega_{pe}) = 4.12 \times 10^{-1}$ stay the same. Such choice means, of course, that magnetic field in Tesla is variable. For example, if we set plasma number density to $n_0 = 10^{15} \text{ m}^{-3}$ (i.e. fix $\omega_{pe} = 1.78 \times 10^9$ Hz radian), this sets Debye length at $\lambda_D = 6.90 \times 10^{-4} \text{ m} = 4.12 \times 10^{-3} c/\omega_{pe}$ and electron Larmor radius at $r_{L,e} = 6.90 \times 10^{-2} \text{ m} = 4.12 \times 10^{-1} c/\omega_{pe}$. Also, then $B_{z0} = 1.01 \times 10^{-4} \text{ T} \approx 1$ gauss. If we set plasma number density to $n_0 = 10^{-5} \text{ m}^{-3}$, this sets Debye length at $\lambda_D = 6.90 \times 10^6 \text{ m} = 4.12 \times 10^{-3} c/\omega_{pe}$ and electron Larmor radius at $r_{L,e} = 6.90 \times 10^8 \text{ m} = 4.12 \times 10^{-1} c/\omega_{pe}$. Also, then $B_{z0} = 1.01 \times 10^{-14}$ Tesla. In other words, appropriately adjusting plasma number density n_0 , physical domain can have arbitrary size e.g. Sun-earth distance (but then unrealistically low density has to be assumed). Since the number of grid points and domain size (normalised to c/ω_{pe}) is set independently, we have to make sure that grid size is $1\lambda_D$ by setting $n_x = 25000$ and $L_{x,max} = 25000 \times \lambda_D = 102.94 c/\omega_{pe}$ and $n_y = 1$ and $L_{y,max} = 1 \times \lambda_D = 4.12 \times 10^{-3} c/\omega_{pe}$. For the velocity we have $(u_x, u_y) = (80, 80)$ grid points with maximal possible velocities for electrons allowed set $u_{x,max} = u_{y,max} = 0.25c$ ($u_{x,max} = u_{y,max} = 0.4c$ in Section 2.3) for electrons and $u_{x,max} = u_{y,max} = 0.25/\sqrt{1836}c = 5.83 \times 10^{-3}c$

for ions. Since the code does not allow to set magnetic field along x -axis (because $\mathbf{B} = (0, 0, B_z)$), to represent the situation adequately, we have only a choice to set a B_{z0} component, which we fix at 0.01 in normalised units. This is not an unreasonable value for, transverse to the considered plasma thread, component of magnetic field above an active region. At first, it seems unrealistic to ignore magnetic field along x . However, firstly, bulk of the work in the quasilinear theory indeed makes the same assumption (ignores longitudinal magnetic field). Secondly, it is known (Alexandrov, Bogdankevich, and Rukhadze, 1988) that in the case of weak fields, general picture of excitation of the Langmuir waves by a low density ($n_b \ll n_e$) electron beam (i.e. their resonant interaction) via Cherenkov resonance is not much different from the case without the magnetic field.

In all presented numerical runs boundary conditions for all quantities are periodic. A typical numerical run takes 32 hours on 256 processor cores (Dual Quad-core Xeon, eight cores per computing node).

We now briefly re-iterate key facts about beam-plasma interaction theoretical framework. In the case without magnetic field (or in the weak field case) cold plasma dispersion relation yields two possible modes (e.g. Alexandrov, Bogdankevich, and Rukhadze, 1988, p.156):

$$\omega^2 = k^2 c^2 + \omega_{pe}^2 + \omega_{pb}^2 \gamma^{-1}, \quad (4)$$

$$1 - \frac{\omega_{pe}^2}{\omega^2} - \frac{\omega_{pb}^2 \gamma^{-3}}{(\omega - k_{\parallel} v_b)^2} \left[1 + \frac{k_{\perp}^2 v_b^2 \gamma^2}{\omega^2} \right] = 0. \quad (5)$$

Here, $\omega_{pb} = \sqrt{n_b e^2 / (\epsilon_0 m_e)}$ the beam plasma frequency and v_b is its speed. γ is the usual Lorentz factor for the bulk motion of the beam (in cold plasma approximation thermal motions of plasma are absent). Note that here only electron and beam contributions are retained whilst ion contribution is ignored due to its smallness. Equation (4) describes a stable, purely transverse ($\mathbf{E} \perp \mathbf{k}$), EM wave which does not interact with the beam because $\mathbf{E} \cdot \mathbf{v}_b = 0$. If $B_0 \parallel z$ then in the *cold* plasma approximation beam can only propagate along z -axis (Note that our numerical simulations are with *finite* temperature). EM wave described by Equation (4) has non zero E_y component only. Equation (5) describes oblique wave which has both $E_{\parallel} = E_z$ and E_x components and hence can interact with the beam via Cherenkov resonance. By putting $\omega = k_{\parallel} v_b + \delta = k_z v_b + \delta$ into Equation (5) growth rates (for $k_{\parallel} v_b \leq \omega_{pe}$ when the oblique mode becomes unstable), δ , can be easily found: (i) away from the plasma frequency, $\omega^2 \approx k_{\parallel}^2 v_b^2 \neq \omega_{pe}^2$ (non-resonant case),

$$\delta_{nr} = \frac{\omega_{pb} \gamma^{-3/2}}{\sqrt{1 - \omega_{pe}^2 / (k_{\parallel}^2 v_b^2)}} \left[\frac{k_{\parallel}^2 + k_{\perp}^2 \gamma^2}{k_{\parallel}^2} \right]^{1/2}, \quad Im(\delta_{nr}) \propto \omega_{pe} \left(\frac{n_b}{n_e} \right)^{1/2} \quad (6)$$

(ii) close to the plasma frequency, $\omega^2 \approx k_{\parallel}^2 v_b^2 \approx \omega_{pe}^2$ (resonant case),

$$\delta_r = \omega_{pe} \left[\frac{n_b}{2n_e} \frac{1}{\gamma^3} \frac{k_{\parallel}^2 + k_{\perp}^2 \gamma^2}{k_{\parallel}^2} \right]^{1/3}, \quad \text{Im}(\delta_r) \propto \omega_{pe} \left(\frac{n_b}{n_e} \right)^{1/3}. \quad (7)$$

Naturally, the resonant growth rate is much larger than the non-resonant one, $\delta_r \gg \delta_{nr}$, due to the beam's low density ($n_b \ll n_e$). As is also clear from Equation (5), the Cherenkov resonance effectively excites Langmuir (longitudinal) waves with the dispersion relation $\omega^2 \approx \omega_{pe}^2$ (note that thermal effects are ignored in Equations (4)-(9)).

In the case of strong magnetic field ($\omega_{ce} \gg \omega_{pe}$) there are two types of waves, dispersion relations of which are given by (Alexandrov, Bogdankevich, and Rukhadze, 1988)■

$$k^2 - \omega^2/c^2 = 0, \quad (8)$$

$$k_{\perp}^2 + \left(k_{\parallel}^2 - \omega^2/c^2 \right) \left(1 - \omega_{pe}^2/\omega^2 - \omega_{pb}^2 \gamma^{-3} / (\omega - k_{\parallel} v_b)^2 \right) = 0. \quad (9)$$

Our Equation (9) without the beam contribution term is also derived by Arons and Barnard,■

1986, their Equation (49), and is referred to as O-mode. The beam does not interact with the purely transverse EM wave given by Equation (8), while it can interact with the slow wave ω_- given by Equation (9) (Equation (9) describes oblique EM waves which have both E_{\parallel} and E_x and in the absence of the beam reduces to the fast (ω_+) and slow (ω_-) modes with dispersion

$$\omega_{\pm}^2 = 0.5 \left[\omega_{pe}^2 + k^2 c^2 \pm \sqrt{(\omega_{pe}^2 + k^2 c^2)^2 - 4\omega_{pe}^2 k_{\parallel}^2 c^2} \right].$$

Electron beam then can resonantly interact with the slow mode when ω_- intersects with $\omega = k_{\parallel} v_b$ line. Thus, the presence of the longitudinal magnetic field can only alter value of k_{\parallel} at which the Cherenkov resonance occurs. It should be stressed that Equations (4)-(9) are derived in the case electron beam propagating strictly along the magnetic field. Therefore, beam is strictly decoupled from the purely transverse EM wave (Equation (8)). If the *beam* has a small k_{\perp} (note that k_{\perp} in Equations (4-9) refers to that of a wave mode) then it can couple to EM wave and hence generate it. This is our main motivation for have small B_{z0} so that when beam is injected along x -axis it can couple to the EM mode. Also, Hsu (2010) showed, using relativistic Vlasov equation, that in unmagnetised plasma, EM and plasma wave conversion efficiency diminishes to zero at both 0° and 90° incidence angles and peaks between $10 - 20^\circ$ depending on plasma temperature. Here degrees refer to angle between wavenumber \mathbf{k} and density gradient direction. Resuming aforesaid we acknowledge that the present numerical model is not suitable for describing the type III solar bursts directly. Ideally, to represent the true physical reality, it would be preferable to set large B_{x0} in addition to small B_{z0} (as in solar wind Parker spiral in the upper solar corona). However, since the VALIS code only solves for $(E_x, E_y, 0)$ and $(0, 0, B_z)$ we have to simply make sure that when the beam is injected along x -axis it can couple to the EM mode in order to capture the essential physics. At the same time we stress that existence of B_{x0} is not a requirement for the generation of type III bursts *per se*, what is essential is to have finite k_{\perp} in the beam so that it couples to the EM wave (here we achieve

this by setting small B_{z0} only). We also note that it was our intension to consider magnetised plasma with the beam injected strictly along the physical domain. In principle, the coupling to EM wave could have been also achieved by switching off the magnetic field altogether and in addition to u_{0x} , setting $u_{0y} = 0.2 - 0.5c$. This would have created a situation with non-zero k_{\perp} too, thus facilitating the coupling of the beam to an EM wave.

VALIS code allows to set any desired number of plasma particle species. Therefore, because we intend to study spatially localised electron beam on top of the inhomogeneous or homogeneous Maxwellian electron-ion plasma, we solve for three plasma species electrons, ions and the electron beam. The dynamics of the three species, which all interact via EM interaction, can be tracked independently in the numerical code. Velocity distribution function for electrons and ions is always set to

$$f_{e,i}(u_x, u_y) = e^{-m_{r,e,i}(u_x^2 + u_y^2)/(2T)}, \quad (10)$$

where $m_{r,e} = 1$ for electrons and $m_{r,i} = 1836$ for ions. When cases with the beam are considered we set the following distribution

$$f_b(u_x, u_y) = \tilde{n}_b e^{-((u_x - 0.2c)^2 + u_y^2)/(2T_b)}. \quad (11)$$

where \tilde{n}_b is normalised beam number density ($\tilde{n}_b = n_b/n_{e0}$) and it is $\tilde{n}_b = 5 \times 10^{-6}$ for low density beam (Section 2.2) and $\tilde{n}_b = 5 \times 10^{-2}$ for the dense beam (Section 2.3). The normalised number density of the background plasma in the homogeneous case (Section 2.2) is $n_0 = 1$. Thermal spread of the electron beam is specified by setting $T_b = 9T = 9.0 \times 10^5 \text{K}$. Note that the beam is injected along the x -axis, transverse to the background magnetic field B_{z0} . Physics of the initiation of the beam is believed to be related to the magnetic reconnection. In 2D case reconnection electric field at a magnetic null is in direction out-of-plane where magnetic field lies. Therefore, it is not unreasonable to consider situation when beam is injected as in our model. Also, beam injection transverse to the magnetic field can result from accelerated electrons from the collapsing magnetic traps (Karlický and Kosugi, 2004). In the inhomogeneous cases (Sections 2.1 and 2.3) background plasma normalised number density is set to

$$n_0(x) = 1 / \left[1 + 10^8 e^{-[(x - L_{x,max}/2)/21]^4} \right] \quad (12)$$

This density profile mimics a factor of 10^8 density drop from the corona $n_0 = 10^{15} \text{ m}^{-3}$ to $n_{AU} = 10^7 \text{ m}^{-3}$ at 1 AU. Because it is known that numerically most precisely implementable boundary conditions are periodic ones this density profile effectively represents mirror-periodic situation when the domain size is doubled, i.e. at $n_0(x = 0) = n_0(x = L_{x,max}) = 1$ while $n_0(x = L_{x,max}/2) = 10^{-8}$. This way "useful" or "working" part of the simulation domain is $0 \leq x \leq L_{x,max}/2$. Spatial width of the density gradient is $L_{IH} \approx 5c/\omega_{pe}$ (see e.g. Figure 7(c), thick solid curve for $90 < x < 95$). When cases with the beam are considered we set its following density profile:

$$n_b(x) = \tilde{n}_b e^{-[(x-5)/3]^4} \quad (13)$$

which means that the beam is injected at $x = 5c/\omega_{pe}$ and its full width at half maximum (FWHM) is also $\approx 5c/\omega_{pe}$ (see Figure 5(c) dotted curve). Plasma beta in this study, based on the above parameters, is set to $\beta = c_s^2/v_A^2 = v_{th,i}^2/v_A^2 = (v_{th,i}/c)^2(\omega_{pi}/\omega_{ci})^2 = 0.17$. (c_s and v_A are sound and Alfvén speeds respectively.) It should be noted that, strictly speaking, pressure balance in the initial conditions is not kept. There are two reasons for this: (i) solar wind is not in "pressure balance" and it is a continually expanding solar atmosphere solution; (ii) plasma beta is small therefore it is not crucial to keep *thermodynamic* pressure in balance (because its effect on total balance is negligible) and the initial background density stays intact throughout the simulation time (see e.g. Figure 7(c), thick solid curve for $90 < x < 95$).

2.1. Larmor drift-unstable case, inhomogeneous plasma without a beam

It is well known that the mode conversion from electrostatic to EM waves near the plasma frequency is possible by linear coupling on a density gradient. Yin *et al.* (1998) examined the mode conversion from electrostatic to EM waves near the plasma frequency in the Earth's electron fore-shock. The conversion and reflection coefficients were obtained by solving coupled differential equations in a weakly magnetised warm plasma with a longitudinal linear density gradient. Results indicated that the fore-shock first harmonic EM emissions and the backward-propagating Langmuir waves required for the generation of the second harmonic EM waves could be efficiently generated by the linear conversion process in an inhomogeneous plasma. Therefore, originally the aim was to study super-thermal beam injection into plasma with homogeneous and inhomogeneous plasma to study the effect of the density gradient on the level of EM wave generation. However, we found originally unforeseen outcome in that with or without electron beam background density gradient regions generate perturbations in all quantities $n(x)$, E_x , E_y and B_z . The results are presented in time-distance plots in Figure (1) and Figures (2)-(3). Dynamical picture is presented in movie 1 in the electronic supplement to this article.

As shown below, the obtained results can be interpreted by means of Larmor-drift unstable mode Alexandrov, Bogdankevich, and Rukhadze, 1988, p.239. Therefore before discussing this numerical run results, let us briefly summarise key facts about the Larmor-drift instability. For frequencies smaller than the Larmor-drift frequency $\omega \leq \omega_{LD} = k_y v_{th,\alpha}^2 / (\omega_{c\alpha} L_{IH})$ this mode is aperiodically unstable in certain regimes (which as we will see below are always taking place in our model). Physical meaning of Larmor-drift in inhomogeneous plasma is clear. When magnetic field is directed along z and plasma inhomogeneity is along x -axis, variation of the particle Larmor radii (due to the inhomogeneity) generates transverse to the both directions current $J_y \approx q_\alpha n_\alpha v_{th,\alpha}^2 / (\omega_{c\alpha} L_{IH})$. This drift is *not* related to the actual motion of centres of the Larmor orbits, and it is preferentially realised in low beta plasmas when particles are magnetised. It is important to note that such Larmor-drift instabilities may occur in Maxwellian plasmas and they are not related to the existence of a positive-sloped region in the velocity distribution function. In this sense the instability can be regarded as hydrodynamic. In the limit of long wavelength approximation, $\lambda_\perp \gg r_{L,i}$,

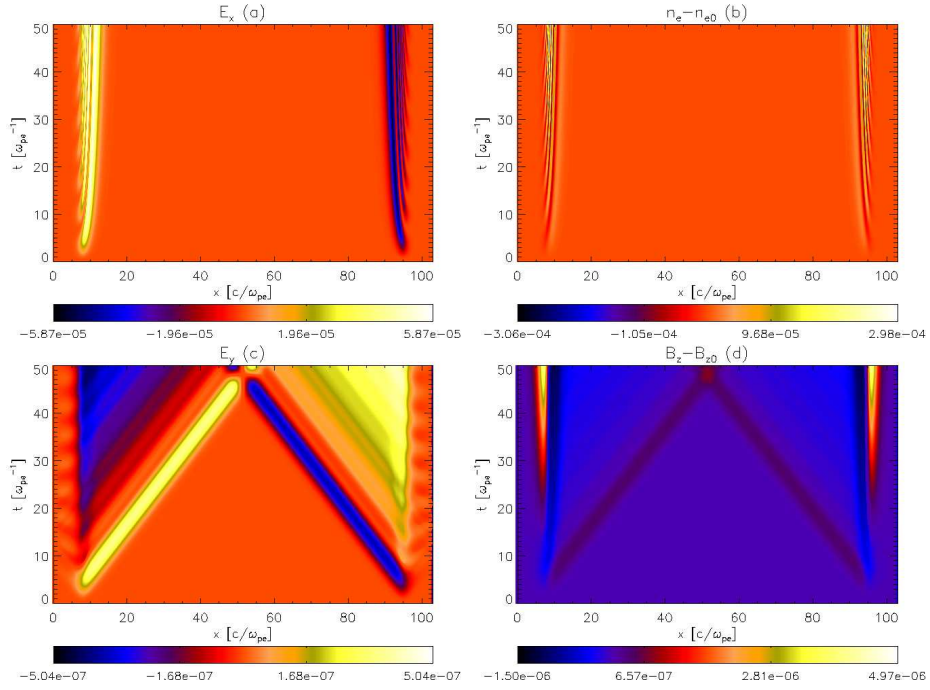


Figure 1. Time-distance plots for: (a) E_x , (b) $n_e - n_{e0}$, (c) E_y and (d) $B_z - B_{z0}$.

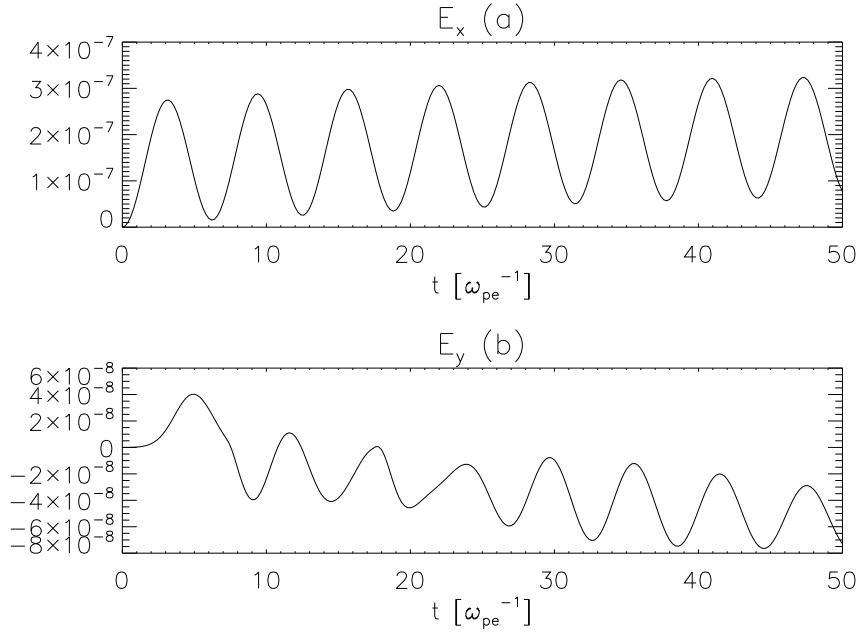


Figure 2. Time evolution of: (a) $E_x(x=5, t)$ and (b) $E_y(x=5, t)$.

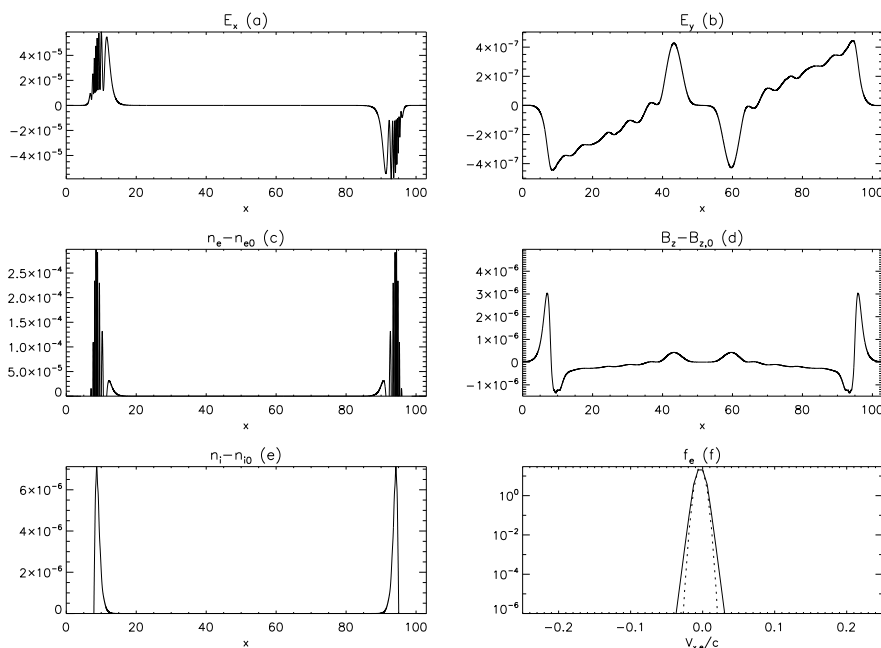


Figure 3. (a) $E_x(x, t = 50)$, (b) $E_y(x, t = 40)$, (c) $n_e(x, t = 50) - n_{e0}$, (d) $B_z(x, t = 40) - B_{z0}$, (e) $n_i(x, t = 50) - n_{i0}$, (f) $f_e(v_x)$. In (f) dotted curve represents $f_e(v_x, t = 0)$ while solid one $f_e(v_x, t = 50)$. For E_y and $B_z - B_{z0}$ the time snapshot $t = 40$ is chosen before the end of the simulation time, $t = 50$, in order to show the spatial profiles before EM fronts collide. It can be seen in Figure 1(c) (look horizontally across $t \approx 50$) that EM fronts collide at about $t \approx 50$.

and $\omega \gg k_z v_{th,e}$, (which naturally holds because in our case $k_z \rightarrow 0$ because our domain size is infinite in z -direction); also when $\omega \ll \omega_{LD}$; $\omega \ll \omega_{ci}$; and $\omega_{pi} \gg \omega_{ci}$ (for our choice of parameters $\omega_{pi}/\omega_{ci} = c/v_A = 4.29 \times 10^3 \gg 1$ and this holds for arbitrary background plasma number density), Rukhadze and Silin (1964) derived following dispersion relation for the Larmor-drift mode

$$\omega^2 = -\omega_{ci}^2 \frac{k_z^2}{k_\perp^2} \frac{T_e}{T_i} \frac{m_p}{m_e} \frac{\partial \ln n_e T_e}{\partial \ln n_i T_i} \quad (14)$$

Here $\partial \ln A / \partial \ln B = (\partial \ln A / \partial x) / (\partial \ln B / \partial x) = (B \partial A / \partial x) / (A \partial B / \partial x)$ notation is used. It is clear that $\omega \ll \omega_{LD}$ and $\omega \ll \omega_{ci}$ conditions hold too (confirming in retrospect) because $k_z \rightarrow 0$. Equation (14) shows that condition for instability is

$$\frac{\partial \ln n_e T_e}{\partial \ln n_i T_i} > 0 \quad (15)$$

which for uniform temperature plasma $T_e = T_i = const$ reduces to $\partial \ln n_e / \partial \ln n_i = 1 > 0$ is always fulfilled when density variation for ions and electrons is the same. Note that the plasma will be drift unstable for both increasing (positive) and decreasing (negative) density gradients because the ratio $\partial \ln n_e / \partial \ln n_i$ will be *always positive* (negative/negative or positive/positive

is positive). So, we conclude that our inhomogeneous plasma set up is always Larmor-drift, aperiodically unstable. It is also interesting to note that (Alexandrov, Bogdankevich, and Rukha p.169 showed that aperiodic instabilities can lead to density filamentation (creating of spatially thin threads). We can indeed see similar filamentary structures in density (and E_x) in Figures 1(a),1(b) and 3(a),3(c).

We gather from Figures 1(a) and 1(b), that E_x and $n_e - n_{e0}$ perturbations travel rather slowly compared to E_y and the fast part of $B_z - B_{z0}$ (dark oblique strips in Figure 1(d)). As can be inferred from Equation (12) and thick solid curve in Figure 7(c) (for $90 < x < 95$), the lengthscale of the background density gradient is $L_{IH} \approx 5c/\omega_{pe}$ which roughly corresponds to the distance travelled by E_x and $n_e - n_{e0}$ perturbations (see e.g. start and end positions of rightmost bright streak in Figure 1(a) or location of the rightmost peaks in Figures 3(a) and 3(c)), i.e. $11 - 6 = 5c/\omega_{pe}$. This distance is travelled in time $50\omega_{pe}^{-1}$. Thus, the phase speed is estimated as $0.1c$. Generally E_x and $n_e - n_{e0}$ perturbations repeat the shape of the density gradient, and other runs (not shown here), with varied density gradient strength, confirm this. E_y perturbation as can be seen from Figure 1(c) travels from the density gradient edges with a speed $\approx c$ (as the slope of dark and bright bands is unity). $B_z - B_{z0}$ (Figures 1(d) and 3(d)) perturbation has two parts: slow moving part that travels with speed $0.1c$ (as in E_x and $n_e - n_{e0}$) and smaller, leading pulses which travel with speed of c . We also gather from 3(f) that electron temperature is slightly increased (i.e. the electron distribution function gets broader at $t = 50\omega_{pe}^{-1}$ (solid curve) compared to $t = 0$ (dotted curve)).

To estimate frequency both of the slow and fast perturbations, we note the number of bright features along e.g. left edge at $x = 5$ in Figure 1(a) which is 7, counting from the first. Note that the density gradient left edge where $n_0 \approx 1$ is at $x = 5$. The frequency estimate can be better done using Figure 2 where we plot $E_x(x = 5, t)$ and $E_y(x = 5, t)$. The estimate is as follows. In Figure 2(a) the time difference between leftmost and rightmost peaks is $\Delta t = 47.2 - 3 = 44.2\omega_{pe}^{-1}$. Thus $7(1/f) = 44.2\omega_{pe}^{-1} = 44.2 \times (2\pi f_{pe})^{-1}$, and $f \simeq f_{pe}$. Similar calculation for Figure 2(b) yields the time difference between leftmost and rightmost peaks is $\Delta t = 47.5 - 5 = 42.5\omega_{pe}^{-1}$. Thus $7(1/f) = 42.5\omega_{pe}^{-1} = 42.5 \times (2\pi f_{pe})^{-1}$, and $f = 1.035f_{pe}$. We therefore conclude that E_x oscillates at local plasma frequency and corresponds to a plasma wave. Whereas E_y perturbations are EM type (escaping radiation) and oscillate just above the plasma frequency $1.035f_{pe}$.

We would like to stress that the generation of perturbations in the considered Larmor drift unstable case is *not* due to the fact that pressure balance is not kept. In our case plasma beta is small, therefore it is not crucial to keep thermodynamic pressure in balance and the initial background density stays intact throughout the simulation time (see e.g. Figure 7(c), thick solid curve for $90 < x < 95$). We have performed numerical runs where temperature was varied as inverse of $n_0(x)$ so that $p_0 = n_0(x)k_B T_0(x) = const$ (B_{z0} is constant throughout this study) yielding perfect total pressure balance – similar approach to pressure balance was adopted by Tsiklauri, Sakai, and Saito (2005). We confirm that even when total pressure balance was kept, Larmor drift instability still developed and physical system behaviour was similar to what is presented here.

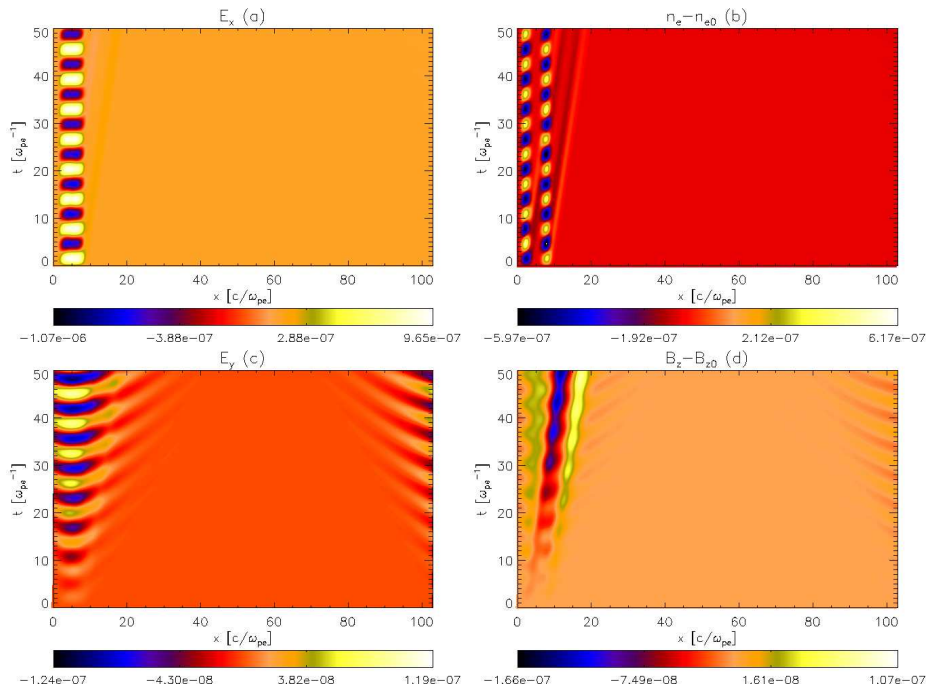


Figure 4. As in Figure 1 but for the case of homogeneous plasma with low density beam.

We note that if finite $B_{0y} = B_{0\perp}$ is added, this will change the Larmor-drift stability criterion. This instability will stabilise if (Rukhadze and Silin, 1964):

$$\frac{B_{0\perp}}{B_{z0}} \geq \frac{v_{th,i}}{\omega_{ci} L_{IH}}. \quad (16)$$

We plan to study this stabilisation issue in a following publication (work in progress), using EPOCH 1.5D particle-in-cell code which allows to choose all background magnetic field components (not as VALIS, which only allows to consider $(E_x, E_y, 0)$ and $(0, 0, B_z)$).

We conclude this subsection with the observation that we found a new possibility for exciting plasma frequency EM radiation by means of a universal, aperiodic Larmor-drift instability. By universal we mean that satisfying the instability criterion (see Equation (14)) is quite plausible in many astrophysical situations. Condition $\omega \ll \omega_{ci}$ requires that $k_z^2/k_\perp^2 \simeq L_\perp^2/L_z^2 \ll m_e/m_p$ i.e. length of the domain should be at least ≈ 43 times longer than its width.

2.2. Plasma emission case, homogeneous plasma with low density beam

To suppress the Larmor-drift instability (because we cannot achieve this by imposing suitable B_{0x}) we now set uniform normalised plasma number density to $n_0 = 1$ and inject a low density beam with the parameters specified above.

The results of this numerical run are presented in Figures 4 and 5, while time dynamics is presented in movie 2 (see the accompanying electronic supplement-

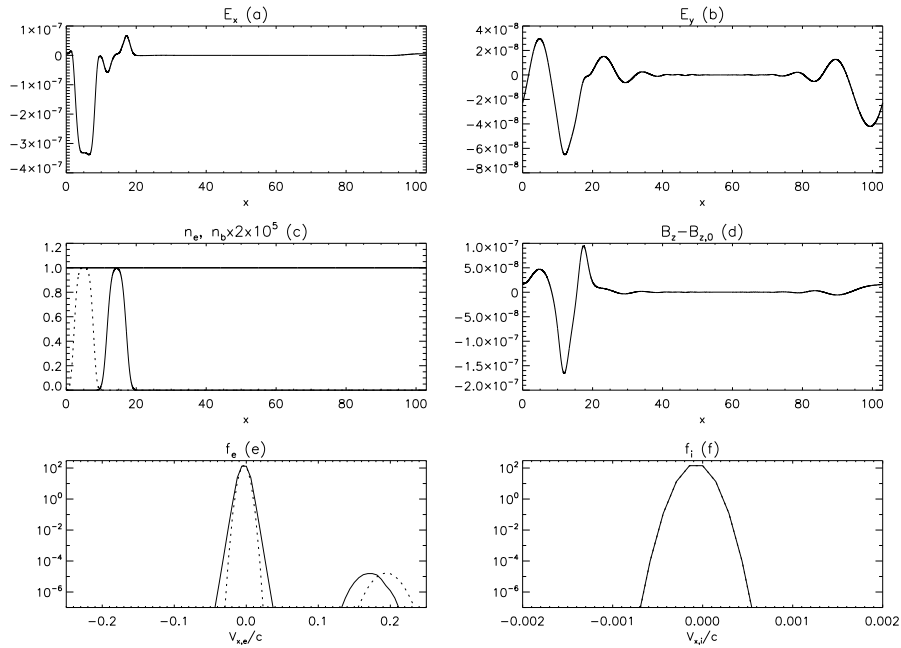


Figure 5. (a) $E_x(x, t = 50)$, (b) $E_y(x, t = 50)$, (c) $n_e(x, t = 50)$ (thick solid horizontal line), $n_b(x, t = 0)$ (dotted curve) and $n_b(x, t = 50)$ (thin solid curve), (note that n_b was scaled by a factor of 2×10^5 to make it visible), (d) $B_z(x, t = 50) - B_{z0}$, (e) $f_e(v_x, t = 0)$ (dotted curve) and $f_e(v_x, t = 50)$ (solid curve), (f) $f_i(v_x, t = 50)$ (solid curve) ($f_i(v_x, t = 0)$ is also plotted with a dotted curve, but to a plotting accuracy the curves overlap, indicating no ion heating takes place).

tary material). One striking novel feature immediately seen in Figures 4(a) and 4(b) (E_x and $n_e - n_{e0}$ where n 's include initially injected beam contribution) is the excitation of standing waves in the spatial location of the beam injection. By counting the number of bright features in the elapsed time, it is clear that the oscillations are at about ω_{pe} . Moreover, E_x oscillates as one solid feature in the spatial location of beam injection (oscillation spatial width coincides with the beam width). While $n_e - n_{e0}$ also exhibits standing waves, but these are in the regions of positive and negative density gradients of the back and front of the *beam* (recall that here background plasma is homogeneous). These oscillations are in anti-phase, i.e. at given $t = const$ over-density and under-density is observed. As with Larmor-drift instability (Section 2.1) this was unforeseen result. However, again literature analysis enabled us to find a suitable interpretation. There are two possible regimes. If the phase of the waves is locked, in the strong instability regime, waves can appear with the frequency close to ω_{pe} in the location of the beam injection (Pavlenko and Petviashvili, 1977). In the case of a weak turbulence regime, the formation of strong Langmuir waves also observed near the beam injection site (Mel'Nik, Lapshin, and Kontar, 1999) (according to their Equation (15) Langmuir turbulence spectral energy density near the beam injection point depends on the phase velocity as $W \propto v^5$). In the electromagnetic E_y and $B_z - B_{z0}$ components (Figures 4(c) and 4(d)) again standing wave at

the beam injection location can be also seen, but in addition this serves as a source to the escaping EM radiation. These can be seen as oblique dark and bright strips with a slope close to unity, thus propagating at about speed of light. Wide dark oblique strip (with narrow bright front) in Figure 4(d) with a slope $\Delta x/\Delta t = (15 - 5)/50 = 0.2$ corresponds to the beam wake (recall that beam travels with speed $0.2c$). Note that in 4(c) and 4(d) there are also EM waves present near $x \approx 100$. This is because the standing wave centred on $x = 5$ generates EM waves travelling in both directions. Because of the periodic boundary conditions, waves that travel to the left, appear on the right side of the simulation domain.

Figure 5 provides further details: 5(a) shows E_x at time $t = 50\omega_{pe}^{-1}$ and is made of two parts (i) a deep centred on $x = 5$ corresponds to the standing wave at plasma frequency and it nicely coincides with beam injection site, see dotted pulse in 5(c) which shows the beam at $t = 0$; (ii) a smaller hump in 5(a) at $x \approx 16$ which roughly coincides with the location to where beam has travelled in time $t = 50\omega_{pe}^{-1}$ (solid pulse in Figure 5(c) centred at $x \approx 15$). Figure 5(e) indicates that bulk plasma electron distribution function heats up (solid peak centred on $v_e = 0$ which corresponds to $t = 50\omega_{pe}^{-1}$ is wider than at $t = 0$). Also we can see that the beam slows down from $0.2c$ to $0.17c$ (small bump (dotted curve) centred at $0.2c$ which represents the beam at $t = 0$ shifts to $0.17c$ (solid curve bump) which is the beam at $t = 50\omega_{pe}^{-1}$). We note that since the beam is nine times hotter than the background plasma, $T_b = 9T = 9.0 \times 10^5 \text{K}$, Larmor radius of the beam is three times larger than that of background plasma, $r_{L,b} = 1.24c/\omega_{pe}$. This is smaller than the distance traveled by the beam ($\approx 10c/\omega_{pe}$ cf. Figure 5(c)). Thus, the beam partial magnetisation can be regarded as the main cause of its slowing down. We also observe that there is no substantial quasilinear relaxation (i.e. plateau does not form) which corroborates basic features of the quasilinear theory. This is due to the fact that the growth rate of resonant Langmuir waves given by Equation (7) is small, as in this run $n_b/n_e = 5 \times 10^{-6}$. A simpler estimate for quasilinear relaxation time, τ , (time of establishing the plateau) is achieved by using $\tau = n_e/(n_b\omega_{pe})$ (e.g. (Mel’Nik, Lapshin, and Kontar, 1999)). Based on this, we see that in our case $\tau = 2 \times 10^5\omega_{pe}^{-1}$. Thus, it is not surprising that in 50 plasma frequencies we do not see substantial quasilinear relaxation. Mel’Nik, Lapshin, and Kontar (1999) quote the criterion of weak turbulence regime of quasilinear theory to apply as $\varepsilon \equiv n_b m_e v_b^2 / (n_0 m_e v_{th,e}^2) \ll 1$. Here, $\varepsilon \approx 10^{-2} \ll 1$, thus we are well in the quasilinear regime. Another interesting corroboration of the quasilinear-theory is that shape of the beam does not change i.e. despite the fact that small density beam plunges through the background plasma at a speed of $0.2c$, it stays intact. Mel’Nik, Lapshin, and Kontar (1999) offer suitable explanation for this fact based on the beam particle kinematics. To avoid duplication we refer the interested reader to this paper for the details. Figure 5(f) confirms that despite the fact ions are treated in the numerical code as moving, still there is no significant change in their velocity distribution function.

It is interesting to note that newly established standing waves can offer an alternative explanation for the horizontal strips observed in some dynamical spectra. Aurass *et al.* (2010) report a narrow-band, short duration line emission

at 314 MHz which is interpreted as a gyro-resonance line. We note that the observed feature can also be explained by an EM emission emanating from the standing waves. This naturally explains the fact that there is no drift in frequency, as the standing wave *remains* in the same spatial location, hence there is no change in density and in emission (plasma) frequency. Moreover, if we look at the dynamical spectra from Figure 1 from Aurass *et al.* (2010) we see that initially, the line intensity increases in time. This behaviour is very similar to what is seen our 4(c) where the intensity increase at $x = 5$ in time can be seen. We can roughly estimate intensity of the line predicted by our model as follows. From Figures 5(b) and 5(d) we can read off typical amplitudes of the escaping EM radiation in the form of standing wave as $E_y \simeq 10^{-7}$ and $B'_z = B_z - B_{z0} \simeq 2 \times 10^{-7}$. Flux of the Poynting vector is than $F = |\mathbf{F}| \simeq E_y B'_z / \mu_0$. Recovering physical units from the normalised quantities yields $F \approx 5 \times 10^{-4} \text{ Wm}^{-2}$. Assuming the area of the emitting source is $A = 20 \text{ Mm} \times 1 \text{ Mm}$ and plasma frequency of $f_p = 300 \text{ MHz}$, we can estimate the flux density at 1 AU as $F_d = FA / [4\pi(1\text{AU})^2 f_p] \approx 1.2 \times 10^{-22} \text{ Wm}^{-2} \text{ Hz}^{-1}$ ($\approx 1 \text{ sfu}$). This is of the order of the Aurass *et al.* (2010) estimate of few sfu for the line flux density.

In summary, the plasma emission case in a homogeneous plasma with low density beam confirms the general picture of quasilinear theory even in the case when the beam is injected *transversely* to the magnetic field, with a main novelty being established that the spatial location where beam is injected serves as a source for standing plasma waves which, in turn, generate escaping EM radiation that oscillates at plasma frequency. This offers a possible new interpretation of the horizontal strips observed in some dynamical spectra.

2.3. Larmor drift-unstable, plasma emission case, inhomogeneous plasma with dense beam

We now combine both effects considered in Sections 2.1 and 2.2 by considering Larmor drift-unstable plasma emission case in which plasma is inhomogeneous and dense beam is injected transverse to the magnetic field and along the density gradient.

We gather from Figure 6(a) that E_x (plasma wave component) now comprises of two parts: a weak standing wave at the location of the beam injection which oscillates with frequency ω_{pe} and a strong wake created by the beam which now shows much more dispersion, as we depart from the quasilinear regime where non-linear interactions between wave modes are ignored. Time-distance plot for $n_e - n_{e0}$ (Figure 6(b) is dominated by a wake created by the beam). EM wave components (E_y and $B_z - B_{z0}$) as in Section 2.2 show similar behaviour where the standing wave centred on $x = 5$ generates escaping EM waves travelling in both directions.

Figure 7(a) shows that E_x has two parts: a small leftmost bump which is from a standing plasma wave and a beam generated perturbation which travels roughly with the beam speed. Figures 7(b) and 7(d) for E_y and $B_z - B_{z0}$, show in more detail, how the standing wave centred on $x = 5$ generates EM waves travelling in both directions with speed of light. We gather from Figure 7(c) that

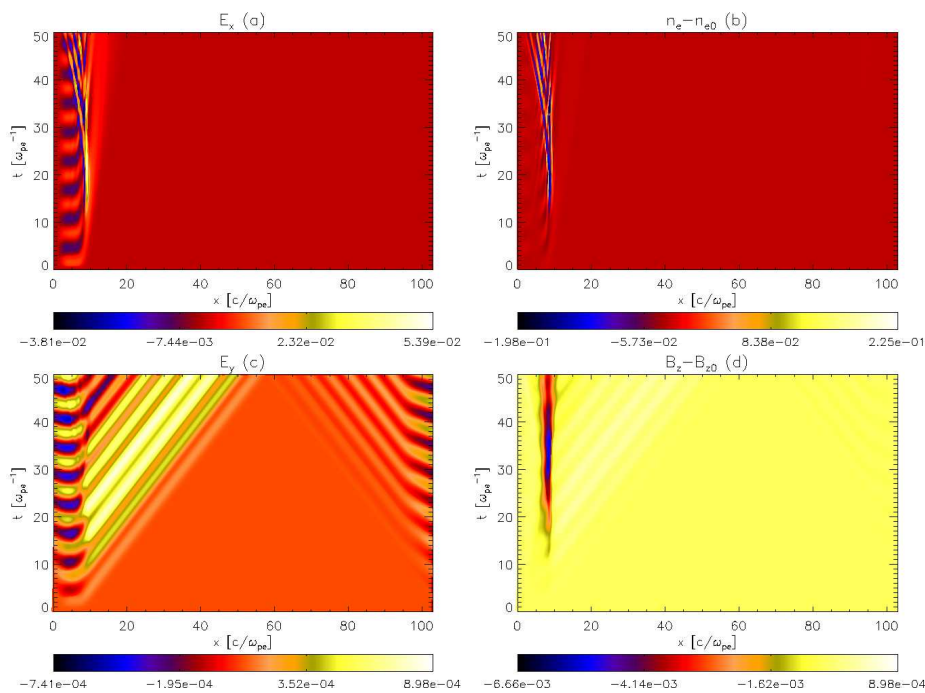


Figure 6. As in Figure 1 but for the case of inhomogeneous plasma with dense beam.

as the dense beam plunges into the plasma, it no longer retains its shape as in quasilinear regime (compare to Figure 5(c)). Figures 7(e) and 7(f) show dynamics of electron and ion distribution functions. We see that as the beam/background plasma number density ratio, $n_b/n_e = 5 \times 10^{-2}$, is no longer small, two effects can be observed: (i) quasilinear relaxation happens very fast; and (ii) substantial electron return current (wide wing with negative velocities in Figure 7(e)) is generated. For ions sizable heating takes place (Figure 7(f)). Dynamical picture of the system evolution can be studied using movie 3 (see the accompanying electronic supplementary material). In the considered case $\tau = 20\omega_{pe}^{-1}$. Thus, it is not surprising that in $50 \omega_{pe}^{-1}$ we see substantial quasilinear relaxation taking place. The criterion of weak turbulence regime $\varepsilon \equiv n_b m_e v_b^2 / (n_0 m_e v_{th,e}^2) \ll 1$ is no longer fulfilled as here $\varepsilon \approx 10^2 \gg 1$. Thus the physical system is not in the quasilinear regime.

In summary, we see for this set of results that the system is driven by the effects of the beam while Larmor-drift effect, whilst present, is not dominant. Significant deviation from the quasilinear theory is found which manifests itself in (i) fast quasilinear relaxation, (ii) disintegration of the beam, and (iii) generation of significant electron return current and ion heating.

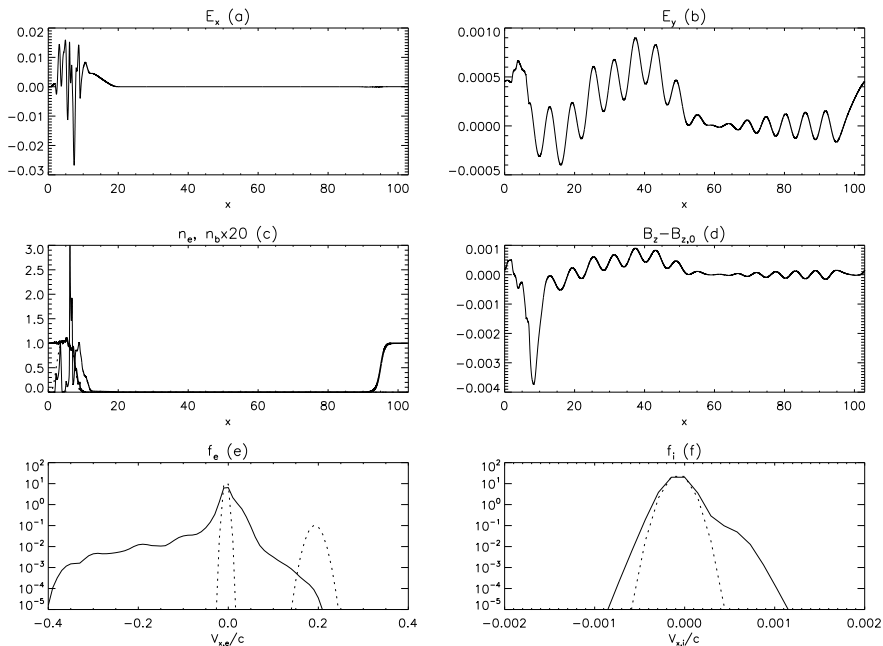


Figure 7. (a) $E_x(x, t = 50)$, (b) $E_y(x, t = 50)$, (c) $n_e(x, t = 50)$ (thick solid curve), $n_b(x, t = 0)$ (dotted curve) and $n_b(x, t = 50)$ (thin solid curve), (note that n_b was scaled by a factor of 20 to make it visible), (d) $B_z(x, t = 50) - B_{z0}$, (e) $f_e(v_x, t = 0)$ (dotted curve) and $f_e(v_x, t = 50)$ (solid curve), (f) $f_i(v_x, t = 0)$ (dotted curve) and $f_i(v_x, t = 50)$ (solid curve).

3. Conclusions

We used 1.5D Vlasov-Maxwell simulations to model EM emission generation in a fully kinetic model for the first time in the solar physics context. We studied plasma emission mechanism and Larmor drift instability in a single plasma thread that joins the Sun to Earth with the spatial scales compressed appropriately. The results can be summarised in three points:

- We established that 1.5D inhomogeneous plasma with a uniform background magnetic field directed transverse to the density gradient is aperiodically unstable to Larmor-drift instability. This instability results in a novel effect of generation of EM emission at plasma frequency. The generated perturbations consist of two parts: (i) non-escaping (trapped) Langmuir type oscillations which are localised in the regions of density inhomogeneity, are highly filamentary, and the period of appearance of the filaments is close to electron plasma frequency in the dense regions; and (ii) escaping electromagnetic radiation with phase speeds close to the speed of light.
- In the uniform density plasma case (when plasma becomes stable to Larmor drift instability), when a *low density* super-thermal, hot beam is injected along the domain, in the direction perpendicular to the magnetic field,

plasma emission mechanism generates non-escaping Langmuir type *standing* oscillations at the beam injection location, which in turn generate escaping electromagnetic radiation at the electron plasma frequency. This result can be used to offer an alternative interpretation to the horizontal strips (usually referred to as the narrowband emission lines in the literature) observed in some dynamical spectra. Quasilinear theory predictions: (i) electron free streaming and (ii) long relaxation time, in accord with the analytic expressions, are confirmed via direct, fully-kinetic simulation.

- We considered interplay of Larmor-drift instability and plasma emission mechanism by studying a *dense* electron beam in the Larmor-drift unstable (inhomogeneous) plasma. We established that in this case the physical system is driven by the effects of the beam while Larmor-drift is not dominant. We also found significant deviation from the quasilinear theory which manifests itself in (i) fast quasilinear relaxation, (ii) disintegration of the beam, and (iii) generation of significant electron return current and ion heating.

We would like to close with the comments in relation to the prospects of comparison of the numerical simulations presented here with the observations (e.g. with the dynamical spectra – 2D radio emission intensity plots where frequency is on y -axis and time on x -axis). Let us base our argument on the level of generated E_y (EM component) in the considered three cases (Sections 2.1-2.3). In the Larmor-drift unstable case without the electron beam according to Figure 1(c) E_y attains values around 5×10^{-7} . In the uniform (Larmor-drift stable case) with a low density beam (see. Figure 4(c)), E_y attains only 10^{-7} (five times less). In the Larmor-drift unstable case with dense beam E_y attains 9×10^{-4} (Figure 6(c)). Based on this we conclude at this stage we cannot produce numerical (synthetic) dynamical spectrum where frequency of the radiation would drop in time as the beam moves along the decreasing density profile. This is for two reasons (i) when we consider small density beam $n_b/n_e = 5 \times 10^{-6}$ (when we are in the quasilinear regime and all known facts about plasma emission mechanism apply) *the beam effect is too small* ($E_y = 10^{-7}$) compared to the Larmor-drift unstable case without the electron beam ($E_y = 5 \times 10^{-7}$), thus there is no point presenting results of Larmor-drift unstable case with weak beam (because Larmor-drift instability overwhelms the effect of the weak beam). (ii) In the Larmor-drift unstable case with dense beam ($n_b/n_e = 5 \times 10^{-2}$), we have $E_y = 9 \times 10^{-4}$, and we do not see decrease of the emission frequency with time because the beam disintegrates in quasilinear time of $\tau = 20\omega_{pe}^{-1}$ (i.e. beam has not enough time to slide down the decreasing density profile) and hence we cannot expect to see plasma emission mechanism in action in its usual form. In summary, the model presented here cannot be directly applied to the type III bursts and it is more relevant for the interpretation of the narrowband line emission observations. In order to simulate the dynamical spectra of type III bursts in which the emission intensity rapidly drifts towards small frequencies in time, as the beam moves to a plasma with decreasing density (and hence ω_{pe}), we would first need to suppress the Larmor-drift instability. In turn, this can be achieved by satisfying the condition set out in Equation (16). However, with the VALIS numerical code this is not possible because it only solves for $(E_x, E_y, 0)$

and $(0, 0, B_z)$. We plan to study this issue further in a following publication (work in progress), using EPOCH 1.5D particle-in-cell code which allows to choose all background magnetic field components. Naturally, PIC method will suffer from the known shortcomings compared to the superior Vlasov-Maxwell approach. However, the benefit of ability of specifying all EM field components outweighs the downsides of the PIC approach.

Acknowledgements The author would like to thank T.D. Arber (Warwick) for useful discussions about VALIS numerical code. Also, useful discussions with E. Kontar (Glasgow) and H. Aurass (AIP) at the CESRA2010 conference are gratefully acknowledged. Computational facilities used are that of Astronomy Unit, Queen Mary University of London and STFC-funded UKMHD consortium at St Andrews University. The author would like to thank HEFCE-funded South East Physics Network (SEPNET) for financial support.

References

- Alexandrov, A., Bogdankevich, L., Rukhadze, A.: 1988, *Foundations of Plasma Electrodynamics (in Russian)*, Moscow: Visshaia Shkola.
- Arons, J., Barnard, J.J.: 1986, Wave propagation in pulsar magnetospheres - Dispersion relations and normal modes of plasmas in superstrong magnetic fields. *Astrophys. J.* **302**, 120–137. doi:10.1086/163978.
- Aurass, H., Rausche, G., Berkebile-Stoiser, S., Veronig, A.: 2010, A microflare with hard X-ray-correlated gyroresonance line emission at 314 MHz. *Astron. Astrophys.* **515**, A1-1-9. doi:10.1051/0004-6361/200913132.
- Cairns, R.: 1985, *Plasma Physics*, Glasgow: Blackie and Son Limited, 124–128.
- Ginzburg, V.L., Zhelezniakov, V.V.: 1958, On the Possible Mechanisms of Sporadic Solar Radio Emission (Radiation in an Isotropic Plasma). *Soviet Astronomy* **2**, 653.
- Hillaris, A., Alissandrakis, C.E., Vlahos, L.: 1988, Dynamics of sub-relativistic electron beams in magnetic traps - A model for solar N-bursts. *Astron. Astrophys.* **195**, 301–309.
- Hillaris, A., Alissandrakis, C.E., Caroubalos, C., Bougeret, J.: 1990, Computation of electron beam parameters for solar type III and J bursts. *Astron. Astrophys.* **229**, 216–223.
- Hillaris, A., Alissandrakis, C.E., Bougeret, J., Caroubalos, C.: 1999, Dynamics of subrelativistic electron beams in the solar corona. Type III group analysis. *Astron. Astrophys.* **342**, 271–278.
- Hsu, J.: 2010, Relativistic theory of mode conversion at plasma frequency. *Physics of Plasmas* **17**(3), 032104. doi:10.1063/1.3322854.
- Kaplan, S.A., Tsytoich, V.N.: 1968, Radio Emission from Beams of Fast Particles under Cosmic Conditions. *Soviet Astronomy* **11**, 956-964.
- Karlický, M., Kosugi, T.: 2004, Acceleration and heating processes in a collapsing magnetic trap. *Astron. Astrophys.* **419**, 1159–1168. doi:10.1051/0004-6361:20034323.
- Kasaba, Y., Matsumoto, H., Omura, Y.: 2001, One- and two-dimensional simulations of electron beam instability: Generation of electrostatic and electromagnetic $2f_p$ waves. *J. Geophys. Res.* **106**, 18693–18712. doi:10.1029/2000JA000329.
- Kontar, E.P., Pécseli, H.L.: 2002, Nonlinear development of electron-beam-driven weak turbulence in an inhomogeneous plasma. *Phys. Rev. E* **65**(6), 066408. doi:10.1103/PhysRevE.65.066408.
- Li, B., Cairns, I.H., Robinson, P.A.: 2008, Simulations of coronal type III solar radio bursts: 1. Simulation model. *J. Geophys. Res.* **113**, 6104. doi:10.1029/2007JA012957.
- Mel’Nik, V.N., Lapshin, V., Kontar, E.: 1999, Propagation of a Monoenergetic Electron Beam in the Solar Corona. *Solar Phys.* **184**, 353–362.
- Melrose, D.B.: 1987, Plasma emission - A review. *Solar Phys.* **111**, 89–101. doi:10.1007/BF00145443.
- Nindos, A., Aurass, H., Klein, K., Trotter, G.: 2008, Radio Emission of Flares and Coronal Mass Ejections. Invited Review. *Solar Phys.* **253**, 3–41. doi:10.1007/s11207-008-9258-9.
- Pavlenko, V.P., Petviashvili, V.I.: 1977, Stability and kinetic effects of a standing Langmuir wave. *JETP Letters* **26**, 200–202.

- Pick, M., Vilmer, N.: 2008, Sixty-five years of solar radioastronomy: flares, coronal mass ejections and Sun Earth connection. *Astron. Astrophys. Rev.* **16**, 1–153. doi:10.1007/s00159-008-0013-x.
- Rhee, T., Ryu, C., Woo, M., Kaang, H.H., Yi, S., Yoon, P.H.: 2009, Multiple Harmonic Plasma Emission. *Astrophys. J.* **694**, 618–625. doi:10.1088/0004-637X/694/1/618.
- Robinson, P.A.: 1992, Clumpy Langmuir waves in type III radio sources. *Solar Phys.* **139**, 147–163. doi:10.1007/BF00147886.
- Robinson, P.A., Cairns, I.H., Gurnett, D.A.: 1992, Connection between ambient density fluctuations and clumpy Langmuir waves in type III radio sources. *Astrophys. J.* **387**, L101–L104. doi:10.1086/186315.
- Rukhadze, A.A., Silin, V.P.: 1964, Reviews of Topical Problems: Method of Geometrical Optics in the Electrodynamics of AN Inhomogeneous Plasma. *Soviet Physics Uspekhi* **7**, 209–229. doi:10.1070/PU1964v007n02ABEH003662.
- Sakai, J.I., Kitamoto, T., Saito, S.: 2005, Simulation of Solar Type III Radio Bursts from a Magnetic Reconnection Region. *Astrophys. J.* **622**, L157–L160. doi:10.1086/429665.
- Sircombe, N.J., Arber, T.D.: 2009, VALIS: A split-conservative scheme for the relativistic 2D Vlasov-Maxwell system. *J. Comp. Phys.* **228**, 4773–4788. doi:10.1016/j.jcp.2009.03.029.
- Smith, D.F.: 1970, Type III solar radio bursts. *Adv. Astron. Astrophys.* **7**, 147–226.
- Tsiklauri, D., Sakai, J., Saito, S.: 2005, Particle-In-Cell simulations of circularly polarised Alfvén wave phase mixing: A new mechanism for electron acceleration in collisionless plasmas. *Astron. Astrophys.* **435**, 1105–1113. doi:10.1051/0004-6361:20042436.
- Umeda, T.: 2010, Electromagnetic plasma emission during beam-plasma interaction: Parametric decay versus induced scattering. *J. Geophys. Res.* **115**, 1204. doi:10.1029/2009JA014643.
- Yin, L., Ashour-Abdalla, M., El-Alaoui, M., Bosqued, J.M., Bougeret, J.L.: 1998, Generation of electromagnetic f_{pe} and $2f_{pe}$ waves in the Earth’s electron foreshock via linear mode conversion. *Geophys. Res. Lett.* **25**, 2609–2612. doi:10.1029/98GL01989.
- Zaitsev, V.V., Mityakov, N.A., Rapoport, V.O.: 1972, A Dynamic Theory of Type III Solar Radio Bursts. *Solar Phys.* **24**, 444–456. doi:10.1007/BF00153387.